https://doi.org/10.5194/egusphere-2026-5656
Preprint. Discussion started: 9 November 2026
© Author(s) 2026. CC BY 4.0 License.

Intercomparison of Four Stomatal Flux-Based Ozone Damage Schemes in CLM5.0 over China: Implications for Carbon, Water, and Energy Fluxes

Xin Lin[1,3], Tiexi Chen[2,3], Xu Yue[4], Shengjie Zhou[2], Sunhao Wang[2]

[1]School of Geographical Sciences, Qinghai Normal University, Xining 810008, Qinghai, China
[2]School of Geographical Sciences, Nanjing University of Information Science and Technology, Nanjing 210044, China
[3]Qinghai Provincial Key Laboratory of Plateau Climate Change and Corresponding Ecological and Environmental Effects, Qinghai Institute of Technology, Xining 810016, China
[4]State Key Laboratory of Climate System Prediction and Risk Management (CPRM), Jiangsu Collaborative Innovation Center of Atmospheric Environment and Equipment Technology, School of Environmental Science and Engineering, Nanjing University of Information Science & Technology (NUIST), Nanjing, 210044, China

Correspondence to: Tiexi Chen (txchen@nuist.edu.cn)

Abstract. Surface ozone (O_3) alters terrestrial carbon–water–energy fluxes. Stomatal flux-based damage schemes nevertheless diverge widely in both impact magnitude and implied carbon–water coupling. Within a unified land surface framework for China, joint comparisons of scheme effects on carbon, water, and energy responses remain limited. Here we couple four stomatal flux-based O_3 damage schemes (Lombardozzi13, Li24, Sitch07, and Ma23) into the Community Land Model version 5.0 (CLM5.0). Using ChinaFLUX sites and regional simulations over China, we compare the schemes at the site, regional, and plant functional type (PFT) scales. The schemes mainly alter the amplitude of simulated fluxes, with little effect on their correlation with observations. Damage intensities differ substantially among schemes. At both site and regional scales, Lombardozzi13 produces the strongest suppression of gross primary productivity (GPP) and transpiration, about 2.4–3.5 times that of the other schemes. Spatial patterns of O_3 impacts are broadly consistent across schemes. Impact fields from Lombardozzi13 and Li24 are more continuous, whereas those from Sitch07 and Ma23 are more concentrated in localised high-value zones. Scheme differences are largest for forest PFTs. Lombardozzi13 overestimates forest damage overall. Li24 suppresses GPP and transpiration in broadleaf forests more strongly than Sitch07 and Ma23, while its responses in needleleaf forests and shrubs resemble those of the latter two. The schemes also alter simulated carbon–water coupling. Li24 yields asynchronous GPP and transpiration responses across vegetation types. By contrast, Sitch07 and Ma23 produce more synchronous responses across most PFTs, except that Ma23 increases grassland sensitivity. These results show that scheme choice controls the magnitude, spatial expression, and carbon–water coupling of ecological O_3 effects. It is therefore a major source of uncertainty in assessing ecological O_3 impacts.

https://doi.org/10.5194/egusphere-2026-5656
Preprint. Discussion started: 9 November 2026
© Author(s) 2026. CC BY 4.0 License.

1 Introduction

Surface ozone (O_3) is a secondary gaseous pollutant formed mainly by photochemical reactions of nitrogen oxides (NO_x) and volatile organic compounds (VOCs) under strong solar radiation. It is now one of the most pressing atmospheric environmental problems globally and in China (Ainsworth et al., 2012; Li et al., 2019; Wang et al., 2017). In recent years, O_3 pollution in China has shown early seasonal onset, wide spatial coverage, and prolonged duration (Lu et al., 2018; Li et al., 2019; Wang et al., 2022). In key regions such as the Yangtze River Delta, the North China Plain, the Pearl River Delta, and the Sichuan Basin, growing-season O_3 concentrations have long exceeded the critical level for plant injury (40 ppb), threatening ecosystem health and regional climate stability (Yue et al., 2017; Mao et al., 2024).

Once O_3 enters mesophyll tissue through stomata, it causes oxidative stress, damages the photosynthetic apparatus, reduces carboxylation efficiency, and accelerates leaf senescence. These effects lower gross primary productivity (GPP) and carbon-sink strength (Krupa and Manning, 1988). O_3 can also induce partial stomatal closure and change the partitioning of evapotranspiration and heat fluxes, thereby disrupting coupled carbon–water–energy cycles and feeding back onto regional weather and climate (Zhu et al., 2022; Lombardozzi et al., 2015). Accurately representing O_3-induced vegetation damage in terrestrial system models is therefore essential for reliable land surface simulations and for assessing regional ecological and climatic risks.

O_3 damage schemes in land surface models fall into two broad classes: exposure-based threshold models (for example, accumulated O_3 exposure over a threshold of 40 ppb, AOT40) and stomatal uptake-based flux–response models. Exposure-based metrics are computationally simple and widely used in policy assessment, but they ignore plant physiological regulation and environmental controls on stomatal conductance, which introduces large uncertainty (Mills et al., 2011; Emberson et al., 2000; Anav et al., 2011). Flux–response schemes are driven by stomatal O_3 flux absorbed by plants and couple stomatal conductance to environmental responses. Because they are more physiologically grounded, they have become the mainstream modelling framework.

Representative stomatal flux schemes include Sitch et al. (2007; hereafter Sitch07), the decoupled scheme of Lombardozzi et al. (2013; hereafter Lombardozzi13), and the more recent schemes of Ma et al. (2023; hereafter Ma23) and Li et al. (2024; hereafter Li24). Lombardozzi13 and Li24 calculate photosynthesis and stomatal conductance independently, which can represent distinct O_3 effects on carbon assimilation and water vapour exchange. Sitch07 and Ma23 instead apply proportional reductions and provide a simpler mechanistic representation. Relative to Lombardozzi13, Li24 revises O_3 flux thresholds and damage response functions using a substantially larger set of O_3 fumigation experiments, improving discrimination among plant functional types (PFTs). Building on Sitch07, Ma23 introduces leaf mass per area (LMA) as a key trait, consolidating empirical parameters into a trait-based framework that reduces parameter redundancy and improves spatial transferability.

Previous studies have coupled these schemes into different land surface platforms (for example, CLM, iMAPLE (Yue et al., 2024), and YIBs). Estimates for China nevertheless diverge strongly, partly because model structure, forcing data, and scheme implementation differ among studies. Jin et al. (2023) reported a 29.23% decline in GPP and a 17.47% reduction in

https://doi.org/10.5194/egusphere-2026-5656
Preprint. Discussion started: 9 November 2026
© Author(s) 2026. CC BY 4.0 License.

transpiration with Lombardozzi13. Zhu et al. (2022) found a 20%–40% decrease in GPP and more than a 20% drop in latent heat flux using WRF-Chem with Noah-MP. Wang et al. (2023), by contrast, obtained much smaller reductions in GPP (5.8%) and transpiration (2.8%) with an optimised O_3 scheme in BEPS. Comparative work also highlights scheme sensitivity: Cao et al. (2024) showed that flux losses under Lombardozzi13 were 2.5–4 times those under Sitch07. Because prior work differs in simulation period, ozone concentration datasets, and host-model configuration, differences among O_3 damage schemes cannot be cleanly separated from background land surface model uncertainty. Recently, Zhou et al. (2026) and Li et al. (2026) conducted systematic inter-scheme comparisons within unified land surface model frameworks at global and China regional scales, respectively, thereby partially reducing the entanglement between intrinsic scheme differences and background model uncertainty. Both studies nevertheless evaluate schemes primarily through GPP and provide little comparative assessment of cross-scheme differences in stomatal controls on transpiration and energy partitioning. A complementary China-focused assessment that jointly diagnoses carbon–water–energy responses and systematically compares the schemes is therefore still needed.

Here, we couple Lombardozzi13, Li24, Sitch07, and Ma23 into a single CLM5.0 framework focused on China. Using observations from representative ChinaFLUX forest, grassland, and cropland sites, we first evaluate the schemes at the site scale and then run regional simulations over China under observation-constrained O_3 forcing. This dual-scale design allows us to assess how the schemes capture terrestrial carbon–water–energy fluxes and to quantify differences in estimated O_3 impacts. The results provide a basis for evaluating ecological effects of surface O_3 in China, refining land surface parameterizations, and informing joint strategies for air-pollution control and ecosystem protection.

2 Data and Methods

2.1 Model Setup

We used the Community Land Model version 5.0 (CLM5.0) to simulate ecosystem energy balance and carbon–water cycling over China. CLM5.0 is the terrestrial component of the Community Earth System Model version 2.2 (CESM2.2) (Lawrence et al., 2019). Photosynthesis follows Farquhar et al. (1980), and stomatal conductance is calculated with the Ball–Berry model (Ball et al., 1987). We adopted the CLM5.0-SP (Satellite Phenology) configuration, which prescribes vegetation phenology from satellite data. This setup focuses on canopy-scale carbon assimilation and transpiration without confounding feedbacks from carbon allocation and vegetation dynamics, and is therefore well suited to assessing direct O_3 effects on ecosystem carbon and water fluxes.

Single-point simulations at each site were driven by in situ surface meteorological observations from 2005 to 2010 at 30 min resolution, matching the model time step. Surface O_3 concentrations for each site were taken from the nearest grid cells of the regional O_3 field. Regional simulations cover continental China (15°N–55°N, 70°E–140°E) at 0.5° × 0.5° resolution, with meteorological forcing and O_3 data spanning 2005–2020. To obtain stable initial conditions, each experiment cycled the

https://doi.org/10.5194/egusphere-2026-5656
Preprint. Discussion started: 9 November 2026
© Author(s) 2026. CC BY 4.0 License.

corresponding forcing fields three times. The first two cycles were used for spin-up, and outputs from the final cycle were analysed.

To quantify O_3 effects on carbon, water, and energy fluxes, we designed five numerical experiments: one control with O_3 damage disabled (OFF) and four experiments that each activate one damage scheme (Lombardozzi13, Li24, Sitch07, or Ma23). For Sitch07, intermediate sensitivity coefficients were used (Yue and Unger, 2015). Relative O_3 impacts were expressed as percentage differences between each damage experiment and OFF, calculated as follows: $Run_{damage} - Run_{OFF})/Run_{OFF} \times 100\%$.

2.2 O_3 Damage Schemes

The four schemes were implemented in CLM5.0 with phytotoxic ozone dose (POD) as the central metric. Each scheme calculates stomatal O_3 uptake and applies PFT-specific sensitivity coefficients to modify photosynthetic rate and stomatal conductance. In outline, stomatal O_3 flux above a prescribed threshold (Y) is accumulated to obtain POD_Y. POD_Y then enters PFT-specific response functions that yield a photosynthesis damage factor (F_v) and a stomatal conductance damage factor (F_g). These factors multiply the net photosynthetic rate (A_n) and stomatal conductance (g_s) from the OFF simulation, yielding the corresponding O_3-modified values used in the damage experiments.

This common POD framework keeps the four schemes comparable within one host model, while allowing structural differences to be isolated. The main contrasts among schemes lie in the uptake flux threshold, the formulation of stomatal O_3 flux, and the functional form of the photosynthetic and stomatal response curves. Lombardozzi13 and Li24 treat photosynthetic and stomatal damage with separate factors, so carbon assimilation and water vapour exchange need not change in proportion. Sitch07 and Ma23 instead impose more tightly coupled reductions. Parameter values and scheme-specific settings are summarised in Table 1.

Table 1. Comparison of parameters among the four ozone damage schemes

	Lombardozzi13	Li24	Sitch07	Ma23
k_{O_3}	1.67	1.51	1.67	1.67
		NT: 0.8	NT: 1.6	
		BT: 1.0	BT: 1.6	
Y	0.8	Shrub: 6.0	Shrub: 1.6	$0.019 \times LMA$
		Grass: 1.6	Grass: 5.0	
		Crop: 0.5	Crop: 5.0	
POD	$F_{O_3} = \frac{[O_3]}{r + \frac{k_{O_3}}{g_p}}$ $U_{Y,t} = \Delta t \times \max(F_{O3,t} - \mathrm{Y}, 0)$ $\mathrm{POD}_{Y,t} = \mathrm{POD}_{Y,t-1} + U_{Y,t} \times 10^{-6}$ $-decay - \mathrm{heal}$	$F_{O_3} = \frac{[O_3]}{r + \frac{k_{O_3}}{g_p}}$ $U_{Y,t} = \begin{cases} \Delta t \times \max(F_{O3,t} - \mathrm{Y}, 0) & daytime \\ 0 & else \end{cases}$ $\mathrm{POD}_{Y,t} = \mathrm{POD}_{Y,t-1}(1 - D_t) + U_{Y,t} \times 10^{-6}$	$F_{O_3} = \frac{[O_3]}{r + [\frac{k_{O_3}}{g_p \times F_v}]}$	$F_{O_3} = \frac{[O_3]}{r + [\frac{k_{O_3}}{g_p \times F_v}]}$
F_v	NT: $F_v = 0.839$ BT: $F_v = 0.8752$ Shrub: $F_v = 0.8752$ Grass: $F_v = 0.802 - 0.0009 \times \mathrm{POD}$	NT: $F_v = 1.005 - 0.0064 \times POD$ BT: $F_v = 0.943 \times \exp(-0.0085 \times POD)$ Shrub: $F_v = 1.0 - 0.0395 \times \ln(POD + 1)$ Grass: $F_v = 1.0 - 0.0021 \times POD$	$F_v = 1 - a_0 \times max\{F_{O_3} - Y, 0\}$; NT: $a_0 = 0.02$ BT: $a_0 = 0.02$ Shrub: $a_0 = 0.01$	$F_v = 1 - \frac{a}{LMA} \times max\{F_{O_3} - Y, 0\}$; $a = 3.5 nmol^{-1} sg$

https://doi.org/10.5194/egusphere-2026-5656
Preprint. Discussion started: 9 November 2026
© Author(s) 2026. CC BY 4.0 License.

	Crop: $F_v = 0.802 - 0.0009 \times POD$	Crop: $F_v = 1.0 - 0.0395 \times \ln(POD + 1)$	Grass: $a_0 = 0.02$ Crop: $a_0 = 0.035$	
	NT: $F_g = 0.7823 + 0.0048 \times POD$	NT: $F_g = (1.0 - 0.0778 \times POD)^{0.8}$		
	BT: $F_g = 0.9125$	BT: $F_g = 0.943 \times \exp(-0.0085 \times POD)$		
F_g	Shrub: $F_v = 0.9125$	Shrub: $F_g = 1.0 - 0.0395 \times \ln(POD + 1)$	$F_g = F_v$	$F_g = F_v$
	Grass: $F_g = 0.7511$	Grass: $F_g = 1.0 - 0.0395 \times \ln(POD + 1)$		
	Crop: $F_g = 0.7511$	Crop: $F_g = 1.005 - 0.169 \times \tanh(POD)$		

Note: k_{O3} = Ratio of leaf resistance for ozone to that for water vapor, Y = Stomatal ozone flux threshold ($nmolm^{-2}s^{-1}$), LMA = Leaf mass per area ($g\ m^{-2}$), $[O_3]$ = Ozone concentration at reference level ($nmol\ m^{-3}$), r = the aerodynamic and boundary layer resistance between the leaf surface and the reference level. ($s\ m^{-1}$), g_p = the leaf conductance for H_2O ($m\ s^{-1}$), F_{O_3} = Stomatal ozone flux ($nmolm^{-2}s^{-1}$), $U_{Y,t}$ = ozone uptake for a single time step（$nmol\ O_3\ m^{-2}$）, $POD_{Y,t}$ = Phytotoxic ozone dose ($nmolm^{-2}$), D_t= leaf senescence/phenology factor, $decay$ = ozone degradation term ($nmolm^{-2}$), $heal$ = ozone repair term ($nmolm^{-2}$), F_v = Ozone suppression factor (fraction of undamaged photosynthesis), F_g = Ozone suppression factor (fraction of undamaged Stomatal conductance), a_0 = PFT-specific area-based ozone sensitivity parameter ($nmol^{-1}sm^2$), a = Unified mass-based ozone sensitivity parameter ($nmol^{-1}sg$), NT = Needle leaf forest, BT = Broadleaf forest.

2.3 Data

2.3.1 Site- and Regional-Scale Model Validation Data

At the site scale, we selected eight China Flux Observation and Research Network (ChinaFLUX) stations spanning forests, grasslands, and cropland. Forest sites were Changbaishan (temperate broadleaf–Korean pine mixed forest, CBS), Qianyanzhou (subtropical coniferous plantation, QYZ), Dinghushan (subtropical evergreen coniferous and broadleaf mixed forest, DHS), and Xishuangbanna (tropical seasonal rainforest, XSBN). Grassland sites were Inner Mongolia (steppe, NMG), Haibei (alpine shrub–meadow, HB), and Dangxiong (alpine meadow, DX). The cropland site was Yucheng (temperate dryland cropland, YC). Together these sites cover a wide range of latitudes, elevations, climates, and vegetation types (Yu et al., 2006; Sun et al., 2006; Hu et al., 2008; Fu et al., 2006; Yu et al., 2008). Station locations are shown in Fig. 1. Meteorological observations and continuous eddy-covariance observations of GPP, sensible heat (H), and latent heat (LE) were obtained from the National Ecosystem Science Data Center, National Science & Technology Infrastructure of China.

For regional evaluation, we used two widely applied flux products. FLUXCOM (Jung et al., 2019, 2020) upscales eddy-covariance observations with meteorological forcing and machine learning to provide spatially continuous carbon and energy fluxes. The Global Land Evaporation Amsterdam Model (GLEAM) provides satellite-based estimates of actual evapotranspiration, transpiration, and soil moisture. We used the monthly GLEAM transpiration product (v4.3a) at 0.25° resolution (Miralles et al., 2011, 2025).

2.3.2 Regional Meteorological Forcing, Surface Ozone Concentration, and LMA Data

Regional simulations were driven by the China Meteorological Forcing Dataset (CMFD, v2.0) (He et al., 2020). CMFD provides continuous near-surface meteorological fields at 3 h temporal and 0.1° spatial resolution. It merges surface observations, satellite products, and reanalysis data, and is widely used for land surface modelling over China. In this study,

https://doi.org/10.5194/egusphere-2026-5656
Preprint. Discussion started: 9 November 2026
© Author(s) 2026. CC BY 4.0 License.

CMFD supplied the atmospheric forcing for the 0.5° regional CLM5.0 experiments over 2005–2020, ensuring consistent meteorological drivers across the OFF and four O_3-damage simulations.

Surface O_3 concentrations for both site and regional simulations were taken from the Hourly and 0.1° resolution Surface Ozone Dataset (HrSOD) over China for 2005–2020 (Zhang et al., 2022). HrSOD was constructed with a long short-term memory (LSTM) network trained on more than six million ground-based observations, together with meteorological, remote-sensing, and socioeconomic predictors. Cross-validation yields $R^2 = 0.72$ and RMSE = 11.71 ppb. Relative to chemical-transport-model O_3 fields that often overestimate summer surface O_3 over China, this observation-constrained product reduces exposure uncertainty for ecological impact assessment. For each ChinaFLUX site, O_3 was extracted from the nearest HrSOD grid cells; the same fields forced the regional experiments. Mean growing-season (May–October) O_3 for 2005–2020 is shown in Fig. 2a. Spatial leaf mass per area (LMA) fields were derived from the specific leaf area (SLA) dataset of Moreno-Martínez et al. (2018), obtained from the TRY Plant Trait Database. LMA was obtained as the reciprocal of SLA and used as the key plant trait required by the Ma23 scheme. The resulting LMA distribution over China is shown in Fig. 2b.

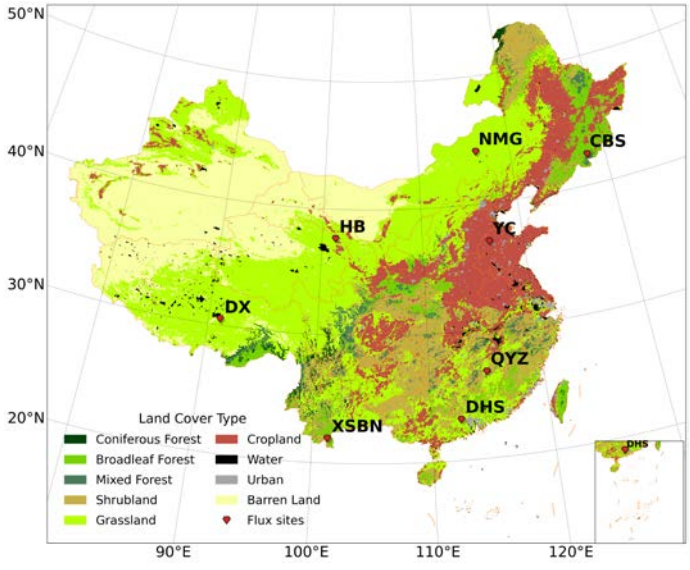


Figure 1. Spatial distribution of land cover types and ChinaFLUX stations

https://doi.org/10.5194/egusphere-2026-5656
Preprint. Discussion started: 9 November 2026
© Author(s) 2026. CC BY 4.0 License.

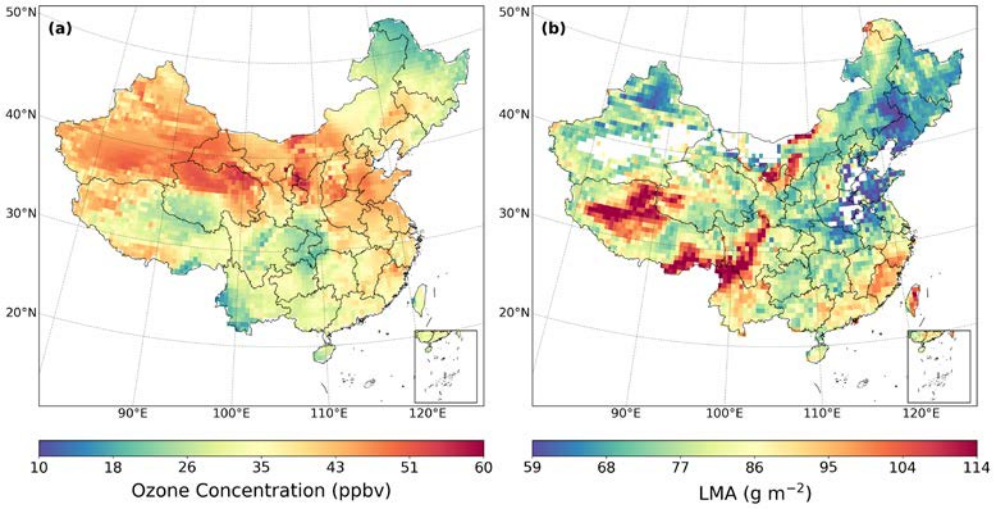


Figure 2. Spatial distributions of (a) surface O_3 concentration and (b) leaf mass per area (LMA) across China.

3 Results

3.1 Model Performance Across O_3 Damage Schemes

Figure 3 shows normalised Taylor diagrams comparing simulated and observed GPP, LE, and H at the eight ChinaFLUX stations after each O_3 scheme was coupled into CLM5.0. In the OFF control, the model reproduced the temporal behaviour of carbon–water–energy fluxes reasonably well. Performance was generally stronger for GPP and LE than for H: the site-averaged Pearson correlation (r) was 0.81 for GPP and 0.74 for both LE and H. Along the normalised root-mean-square distance (RMSD) arcs, LE markers lay closer to the observation reference than H markers of similar r, indicating a better match in amplitude as well as timing for latent heat.

Performance differed among vegetation types. For GPP, forest sites (CBS, DHS, QYZ, and XSBN) outperformed grassland (HB, DX, and NMG) and cropland (YC) sites, with forest r values of 0.73–0.91 and smaller RMSD. At these forests, GPP and LE markers typically clustered at high r (often near or above ~0.8) with normalised standard deviations (SD) mostly below the observation arc (SD = 1), indicating preserved seasonality but somewhat muted variability. Forests also showed the weakest H skill among vegetation categories: H correlations were often lower than those of GPP and LE, and at some sites (notably XSBN) normalised H SD approached or exceeded the observation reference, pointing to larger amplitude errors in sensible heat.

At grassland and cropland sites, normalised SDs of GPP and LE were markedly lower than observed (frequently well below ~0.7), indicating underestimated variability even when temporal correlations remained moderate to high. LE retained relatively strong synchrony at several non-forest sites (for example DX), yet still sat inward of the observation arc on the SD axis. Together, these patterns show that CLM5.0 captured flux timing more faithfully than flux magnitude, especially outside forests.

https://doi.org/10.5194/egusphere-2026-5656
Preprint. Discussion started: 9 November 2026
© Author(s) 2026. CC BY 4.0 License.

Across the four O_3 schemes, correlations of simulated GPP, LE, and H with observations remained largely unchanged relative to OFF: for a given flux and site, scheme markers aligned along nearly the same radial r ray. In contrast, normalised SD decreased to varying degrees, so points shifted toward the origin along that ray. O_3 damage therefore mainly dampened flux amplitude without altering temporal synchrony. Lombardozzi13 produced the largest SD reductions and consistently lay closest to the origin within each colour cluster. Li24, Ma23, and Sitch07 had more moderate, mutually similar effects, occupying intermediate positions between OFF and Lombardozzi13.

Figure 4 shows percentage changes in root-mean-square error (RMSE) for GPP, H, and LE under each O_3 scheme relative to OFF. Positive values indicate degraded accuracy; negative values indicate improvement. Scheme effects on accuracy varied strongly by vegetation type and variable. All schemes increased RMSE at the cropland site (YC), and the increases were largest for GPP. Lombardozzi13 produced the strongest degradation across fluxes; Li24, Ma23, and Sitch07 raised RMSE more moderately and with broadly similar magnitudes. For H and LE at cropland, the same ranking held: Lombardozzi13 caused the largest rise, while the three milder schemes remained closer to the OFF baseline.

At forest sites, the pattern for GPP diverged from that for energy fluxes. Li24, Ma23, and Sitch07 slightly reduced GPP RMSE relative to OFF, with Li24 showing the largest reduction (1.7%). Lombardozzi13 instead increased forest GPP RMSE. For H and LE, however, all schemes increased RMSE: Li24 raised H and LE errors more than Sitch07 and Ma23, and approached Lombardozzi13 for H, so the modest GPP improvement under Li24 did not extend to the heat fluxes. Error bars were large for several forest GPP contrasts, spanning both signs for some schemes, which limits how firmly the small GPP gains can be interpreted. At grassland sites, Lombardozzi13 again increased RMSE for GPP, H, and LE, though less than at cropland. Effects of Li24, Ma23, and Sitch07 remained marginal and near zero for all three fluxes.

Site-averaged across vegetation types, Lombardozzi13 raised RMSE of GPP, H, and LE by 5.8%, 2.8%, and 2.6%, respectively. Li24, Ma23, and Sitch07 generally produced smaller and more similar changes. Together with the Taylor diagrams (Fig. 3), these results show that O_3 schemes leave temporal correlations close to OFF while changing error magnitude (and thus bias or amplitude mismatch) to different degrees. Lombardozzi13 perturbs the simulations most strongly; Li24, Ma23, and Sitch07 have weaker and more similar effects, with only limited, vegetation-specific benefits for forest GPP RMSE.

https://doi.org/10.5194/egusphere-2026-5656
Preprint. Discussion started: 9 November 2026
© Author(s) 2026. CC BY 4.0 License.

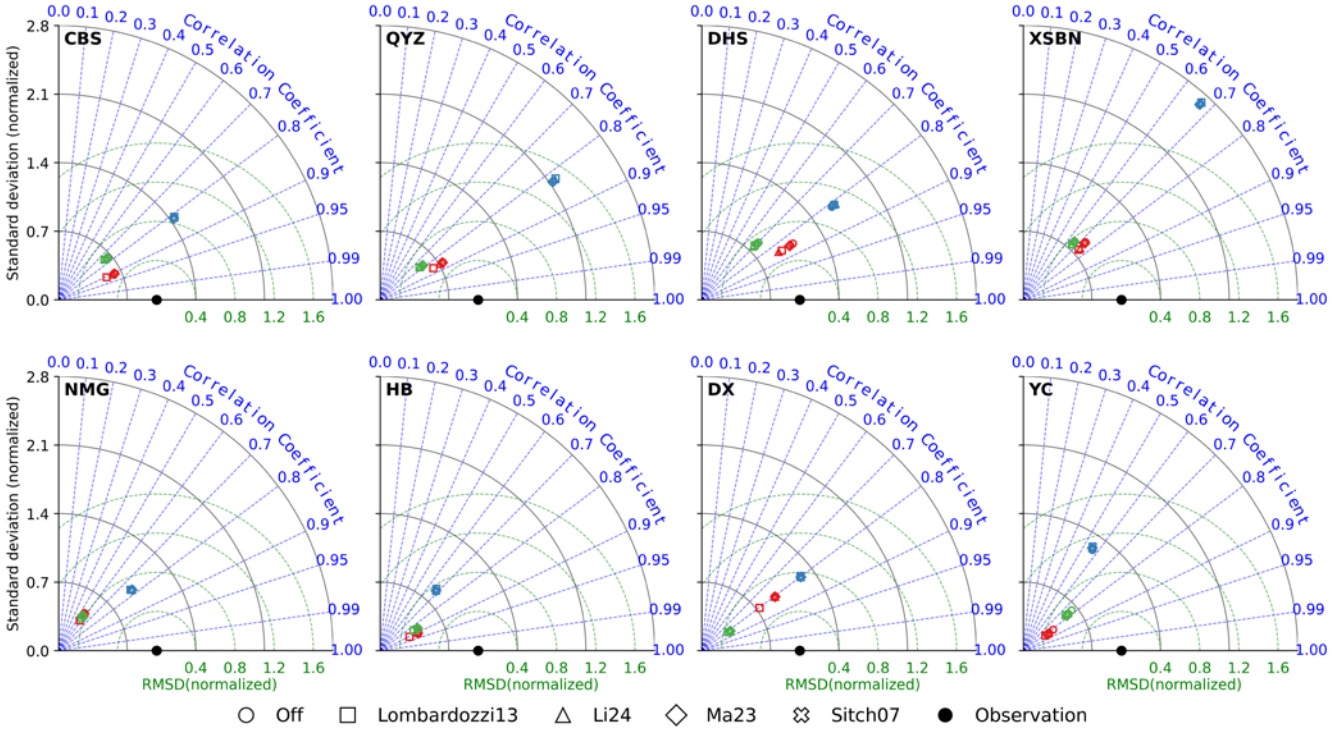


Figure 3. Taylor diagrams comparing simulated and observed GPP, H, and LE fluxes across ChinaFLUX stations. Red, blue, and green symbols denote GPP, H, and LE, respectively.

205

https://doi.org/10.5194/egusphere-2026-5656
Preprint. Discussion started: 9 November 2026
© Author(s) 2026. CC BY 4.0 License.

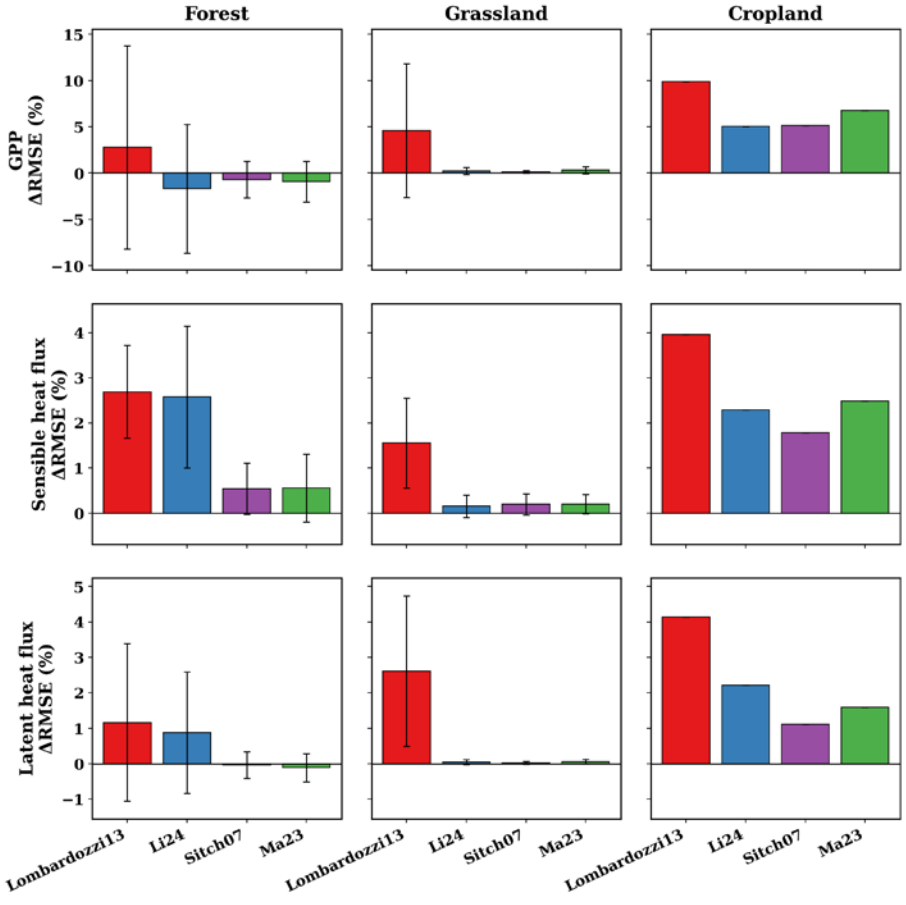


Figure 4. Percentage changes in root-mean-square error (RMSE) under different O_3 damage scenarios relative to OFF.

Regional performance was evaluated against FLUXCOM products for GPP, H, and LE, and against GLEAM for transpiration, using multi-year means for 2005–2020. Under the OFF scenario, CLM5.0 reproduced the dominant spatial gradients of carbon, water, and energy fluxes over China (Fig. 5). GPP, transpiration, and LE increased from the arid northwest toward humid southeastern China, whereas H was higher over the Tibetan Plateau and arid to semi-arid western China and lower in humid southeastern regions. These patterns matched the reference products in sign and large-scale structure.

Relative to the benchmarks, CLM5.0 underestimated GPP, transpiration, and LE most clearly in humid southern China, where the reference fields showed stronger high-flux cores than the simulations. In contrast, H was slightly overestimated over the Tibetan Plateau and western China. Outside these bias hotspots, the model still captured the southeast–northwest contrast that organises the national flux fields.

Spatial statistics confirmed strong spatial consistency between CLM5.0 and the references across O_3 scenarios (Fig. 6). R^2 was highest for GPP (0.90 in all scenarios), followed by LE (0.88–0.89) and transpiration (0.78–0.79); H was lowest (0.67–0.69). Relative bias (RB) indicated systematic underestimation of GPP (−26.9% to −41.1%), transpiration (−33.7% to −41.6%), and LE (−24.4% to −27.1%), together with slight overestimation of H (4.0% to 6.5%). Normalised RMSE (nRMSE) was larger

https://doi.org/10.5194/egusphere-2026-5656
Preprint. Discussion started: 9 November 2026
© Author(s) 2026. CC BY 4.0 License.

for transpiration (0.59–0.64) and GPP (0.44–0.62) than for H (0.36–0.38) and LE (0.37–0.40). Thus spatial pattern agreement was strongest for GPP and LE, whereas magnitude errors were largest for GPP and transpiration.

O_3 parameterization had little effect on spatial correlation: R^2 differed by no more than 0.02 among schemes for any variable. Error magnitudes changed more clearly. Lombardozzi13 produced the largest errors, with nRMSE of 0.62, 0.64, 0.38, and 0.40 for GPP, transpiration, H, and LE, respectively, and the most negative RB for GPP (−41.1%) and transpiration (−41.6%). Li24, Sitch07, and Ma23 performed more similarly to one another and closer to OFF. Among these three, Li24 showed slightly higher nRMSE and RB than Sitch07 and Ma23, which differed only marginally. Overall, O_3 scheme choice altered bias and error amplitude more than the spatial ranking of model–observation agreement.

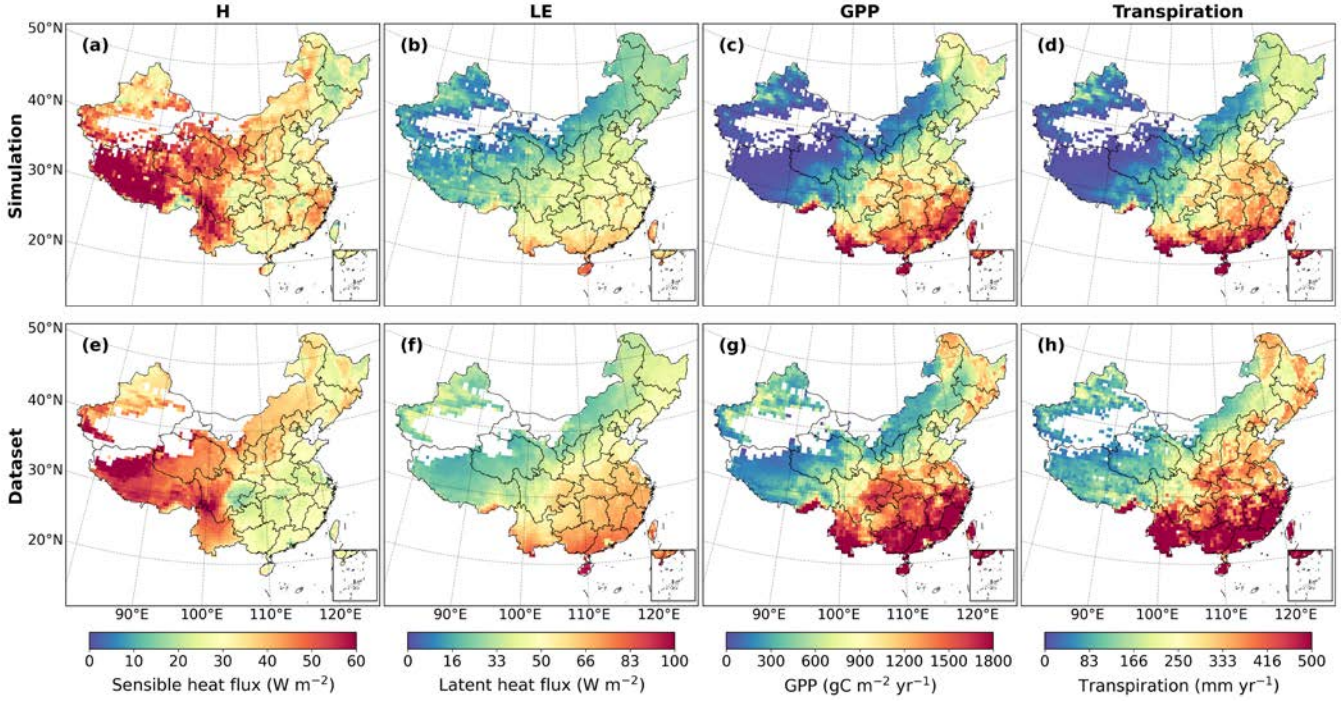


Figure 5. Spatial distributions of multi-year mean GPP, transpiration, H, and LE for 2005–2020. Panels (a), (b), (c), and (d) show CLM5.0 simulations; panels (e), (f), and (g) show FLUXCOM references for GPP, H, and LE; panel (h) shows GLEAM transpiration.

https://doi.org/10.5194/egusphere-2026-5656
Preprint. Discussion started: 9 November 2026
© Author(s) 2026. CC BY 4.0 License.

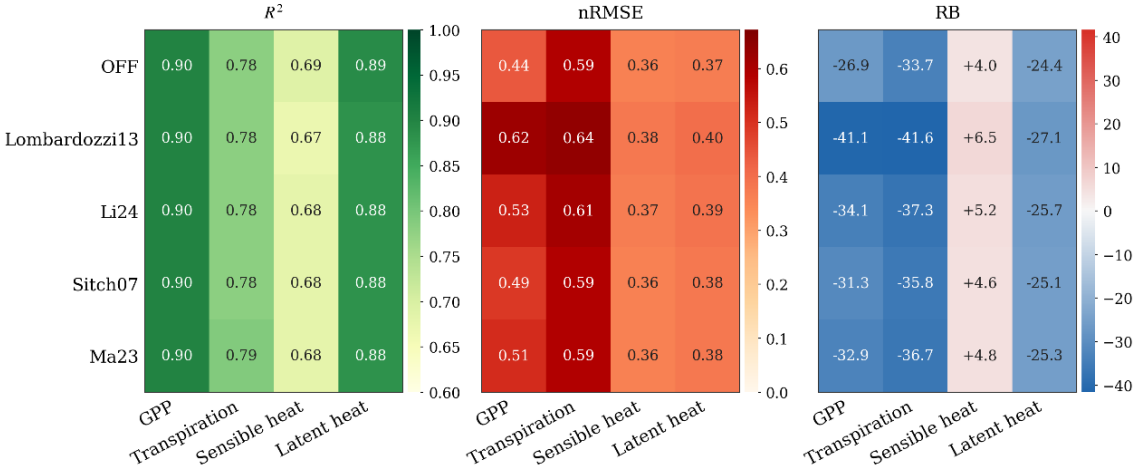


Figure 6. Statistical evaluation of CLM5.0 against reference datasets under different O_3 damage scenarios: (a) R^2, (b) nRMSE, and (c) RB. Columns are variables; rows are scenarios (OFF, Lombardozzi13, Li24, Sitch07, and Ma23).

3.2 Comparison of Simulated Site-Scale Ozone Impacts Among Damage Schemes

Percentage impacts of O_3 on site-scale GPP, LE, and H were calculated from damage-minus-OFF differences at eight flux stations (Table 2). Across all stations and schemes, O_3 reduced GPP and LE and increased H. Percentage impacts on GPP were larger than those on LE and H, and the inter-scheme standard deviation of GPP reduction was also larger (typically ~5–10% for GPP versus ~1–4% for H and LE). Thus carbon flux responded more strongly, and more uncertainly across schemes, than the surface energy fluxes.

For GPP, Lombardozzi13 produced the strongest suppression at all stations except DHS, with a multi-site mean reduction of 16.82%, compared with 6.14% (Li24), 2.56% (Sitch07), and 3.30% (Ma23). Site-level Lombardozzi13 reductions ranged from −11.52% at XSBN to −24.72% at YC. At DHS, Li24 (−15.63%) exceeded Lombardozzi13 (−14.91%), making this the only forest station where the scheme ranking reversed. Across the four forest sites, Li24 (8.37%) exceeded Sitch07 (1.50%) and Ma23 (1.53%). At grassland sites, Li24, Sitch07, and Ma23 averaged only 0.71%, far below Lombardozzi13 (18.57%), so inter-scheme GPP spread was larger for grasslands than for forests. All four schemes projected large GPP reductions at the cropland site YC (scheme mean −17.17%), where Sitch07 and Ma23 also reached double-digit losses (−13.30% and −17.22%). For H, all schemes showed an O_3-driven increase. Lombardozzi13 again gave the largest multi-site mean increase (4.40%), except at DHS, exceeding Li24 (3.28%), Sitch07 (1.19%), and Ma23 (1.49%). At DHS, Li24 increased H by 10.79%, above Lombardozzi13 (7.59%). Li24 exceeded Sitch07 and Ma23 at forest sites, while the three milder schemes were nearly identical at grassland sites, where Sitch07 and Ma23 remained close to zero. Mean H increases were largest at YC (6.39%) and DHS (6.36%). For LE, all schemes showed declines, with inter-scheme contrasts similar to those for H: Lombardozzi13 reductions were widespread (about −2% to −7%), Li24 was strongest among the milder schemes at DHS and YC, and Sitch07 and Ma23

https://doi.org/10.5194/egusphere-2026-5656
Preprint. Discussion started: 9 November 2026
© Author(s) 2026. CC BY 4.0 License.

remained weak at grasslands but stronger at YC. Overall, scheme divergence was organised by plant functional type, with grasslands amplifying GPP disagreement and the cropland site producing the most consistent multi-scheme signal.

Table 2. Percentage impacts of ozone on GPP, H, and LE simulated by four O_3 damage schemes at eight flux stations.

	site	Lombardozzi13/%	Li24/%	Sitch07/%	Ma23/%	Mean/%	Standard Deviation/%
GPP	CBS	−14.66	−3.95	−0.89	−0.71	−5.05	6.58
	QYZ	−15.38	−4.48	−0.75	−0.50	−5.28	6.98
	DHS	−12.56	−15.63	−3.28	−3.96	−8.86	6.18
	XSBN	−11.52	−9.40	−1.06	−0.96	−5.73	5.52
	NMG	−15.60	−0.91	−0.59	−1.68	−4.70	7.29
	HB	−21.87	−1.10	−0.60	−1.33	−6.22	10.43
	DX	−18.25	−0.18	−0.02	−0.01	−4.60	9.10
	YC	−24.72	−13.44	−13.30	−17.22	−17.17	5.35
H	CBS	3.19	1.65	0.28	0.24	1.34	1.40
	QYZ	6.09	4.18	0.38	0.27	2.73	2.88
	DHS	7.59	10.79	3.18	3.89	6.36	3.53
	XSBN	4.27	4.27	0.61	0.57	2.43	2.12
	NMG	0.91	0.04	0.02	0.06	0.26	0.44
	HB	3.34	0.06	0.07	0.10	0.89	1.63
	DX	1.19	0.00	0.00	0.01	0.30	0.60
	YC	8.59	5.25	4.96	6.76	6.39	1.66
LE	CBS	−4.27	−2.24	−0.37	−0.33	−1.80	1.87
	QYZ	−5.35	−3.66	−0.33	−0.24	−2.40	2.53
	DHS	−4.07	−5.78	−1.70	−2.08	−3.41	1.89
	XSBN	−3.77	−3.77	−0.54	−0.51	−2.15	1.88
	NMG	−2.28	−0.06	−0.05	−0.15	−0.63	1.10
	HB	−7.42	−0.17	−0.18	−0.29	−2.01	3.60
	DX	−3.98	−0.00	−0.02	−0.01	−0.99	1.99
	YC	−7.28	−4.46	−4.24	−5.78	−5.44	1.40

3.3 Spatial Distributions of Regional Ozone Impacts Simulated by Different Damage Schemes

Figure 7 compares O_3 effects on sunlit (PSNSUN) and shaded (PSNSHA) leaf photosynthetic rates relative to OFF. All schemes showed strong inhibition over eastern China, including northeastern China, northern China, and the Sichuan Basin, and weaker effects over northwestern China and the Tibetan Plateau. Reductions under Lombardozzi13 and Li24 were spatially

https://doi.org/10.5194/egusphere-2026-5656
Preprint. Discussion started: 9 November 2026
© Author(s) 2026. CC BY 4.0 License.

more continuous across the eastern half of China, whereas high-reduction zones under Sitch07 and Ma23 were more localised, mainly in northeastern China, northern China, and the Sichuan Basin.

Nationally, Lombardozzi13 yielded the strongest photosynthetic damage, with PSNSUN and PSNSHA decreasing by 15.52% and 13.83%. Ma23 followed for sunlit leaves (11.12%) but showed a much smaller shaded-leaf reduction (4.48%). Li24 and Sitch07 were closer to each other: PSNSUN decreased by 7.07% and 7.40%, and PSNSHA by 4.16% and 3.35%. Across schemes, sunlit-leaf photosynthesis declined more than shaded-leaf photosynthesis. Lombardozzi13 produced relatively similar sunlit and shaded damage (difference of 1.69 percentage points), whereas Li24, Sitch07, and Ma23 suppressed sunlit leaves more strongly. The sunlit–shaded contrast was largest under Ma23 (6.64 percentage points) and Sitch07 (4.05 percentage points), and intermediate under Li24 (2.91 percentage points).

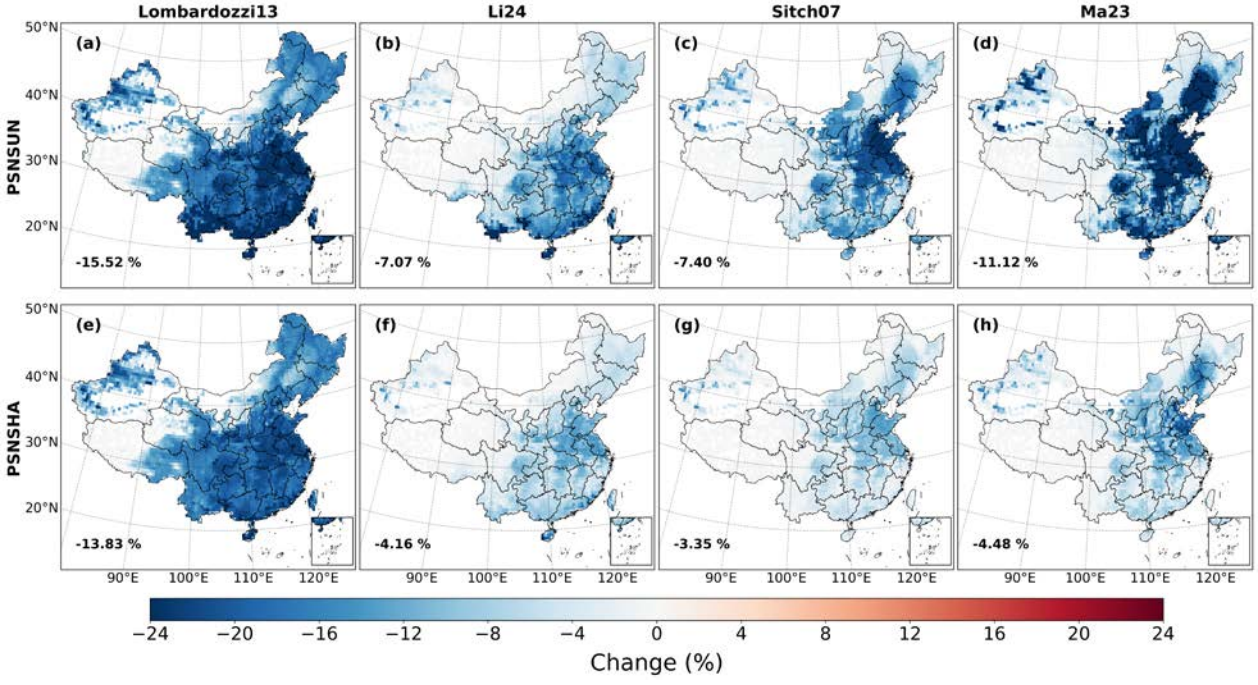


Figure 7. Spatial distributions of changes in sunlit (PSNSUN) and shaded (PSNSHA) leaf photosynthetic rates under different O_3 damage scenarios. Bottom-left values are regional means over China relative to OFF.

Figure 8 further shows how the four ozone damage schemes affected stomatal conductance of sunlit (GSSUN) and shaded (GSSHA) leaves. As for photosynthetic rate in Fig. 7, the schemes differed substantially in response magnitude. Lombardozzi13 produced the strongest stomatal suppression, with GSSUN and GSSHA decreasing by 16.75% and 18.31%, respectively. Ma23 followed (12.82% and 7.03%), then Sitch07 (8.50% and 5.09%) and Li24 (4.26% and 1.39%).

Sunlit and shaded responses also differed among schemes. Under Lombardozzi13, the GSSHA reduction slightly exceeded that of GSSUN. By contrast, Li24, Sitch07, and Ma23 all reduced GSSUN more than GSSHA. Ma23 showed the largest sunlit–shaded contrast among the four schemes. Overall, the canopy vertical pattern of stomatal conductance depended strongly on the damage parameterization.

https://doi.org/10.5194/egusphere-2026-5656
Preprint. Discussion started: 9 November 2026
© Author(s) 2026. CC BY 4.0 License.

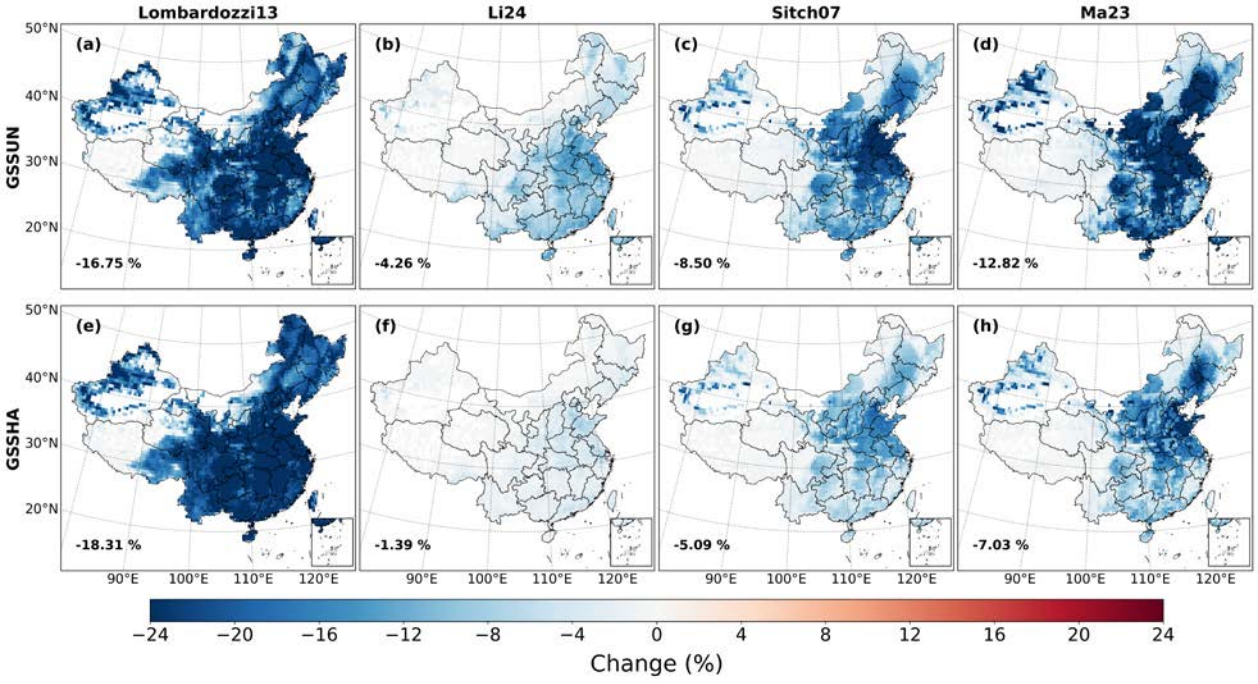


Figure 8. Same as Fig. 7, but for sunlit (GSSUN) and shaded (GSSHA) leaf stomatal conductance.

Figure 9 shows percentage impacts on GPP and ecosystem transpiration relative to OFF. Nationally, Lombardozzi13 produced the largest declines (GPP −15.14%; transpiration −10.65%). For GPP, Ma23 (−7.00%) and Li24 (−6.46%) were similar and exceeded Sitch07 (−4.95%). For transpiration, Li24 (−3.73%) and Ma23 (−3.40%) likewise exceeded Sitch07 (−2.34%). Suppression was concentrated in eastern China, consistent with the photosynthetic and stomatal responses in Figs. 7 and 8, whereas northwestern China and the Tibetan Plateau showed weak changes.

Scheme-wise spatial structure differed. Lombardozzi13 and Li24 produced smoother, more extensive GPP reductions over northern, southern, and parts of southwestern China. Sitch07 and Ma23 instead concentrated GPP damage hotspots over the North China Plain and northeastern agricultural zones, with Ma23 showing darker local cores than Sitch07. Transpiration reductions followed the same east–west contrast but were spatially less heterogeneous and consistently smaller in percentage terms than GPP reductions (national GPP losses exceeded transpiration losses by about 4.5–5.3 percentage points under Lombardozzi13, Ma23, and Li24, and by 2.61 percentage points under Sitch07).

https://doi.org/10.5194/egusphere-2026-5656
Preprint. Discussion started: 9 November 2026
© Author(s) 2026. CC BY 4.0 License.

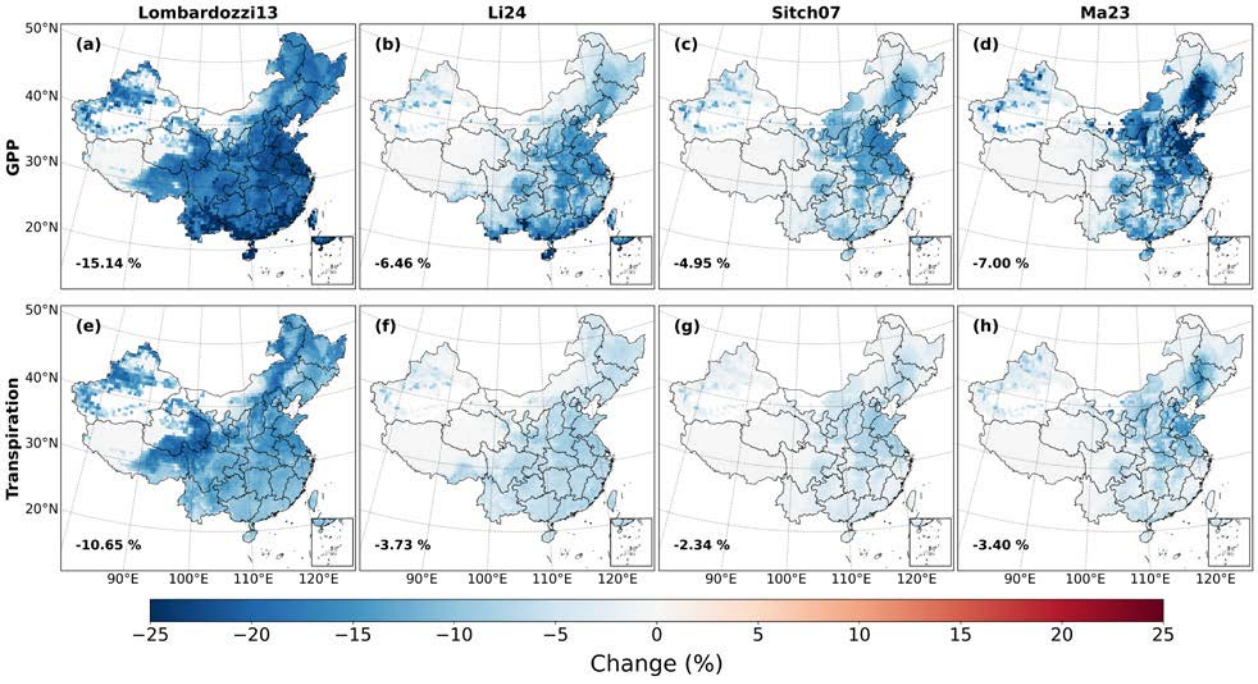


Figure 9. Same as Fig. 7, but for GPP and transpiration.

Reduced transpiration decreased LE and increased H (Fig. 10). Spatial patterns of these percentage impacts broadly followed the transpiration changes in Fig. 9, with the strongest signals again over eastern China. Lombardozzi13 showed the most extensive LE reductions and H increases. Li24 produced comparatively continuous eastern-China changes, whereas Sitch07 and Ma23 remained more regionally clustered over the North China Plain, northeastern China, and related agricultural zones. In each scheme, areas of LE decline coincided spatially with areas of H increase.

Nationally, Lombardozzi13 yielded the largest LE decrease and H increase (−3.07% and +2.99%). Li24 (−1.42% and +1.63%) and Ma23 (−1.09% and +1.13%) were similar and exceeded Sitch07 (−0.81% and +0.88%). Absolute percentage impacts on LE and H were smaller than those on GPP and transpiration, indicating that O_3-driven carbon and water-flux losses translate into more moderate redistributions of the surface energy balance.

https://doi.org/10.5194/egusphere-2026-5656
Preprint. Discussion started: 9 November 2026
© Author(s) 2026. CC BY 4.0 License.

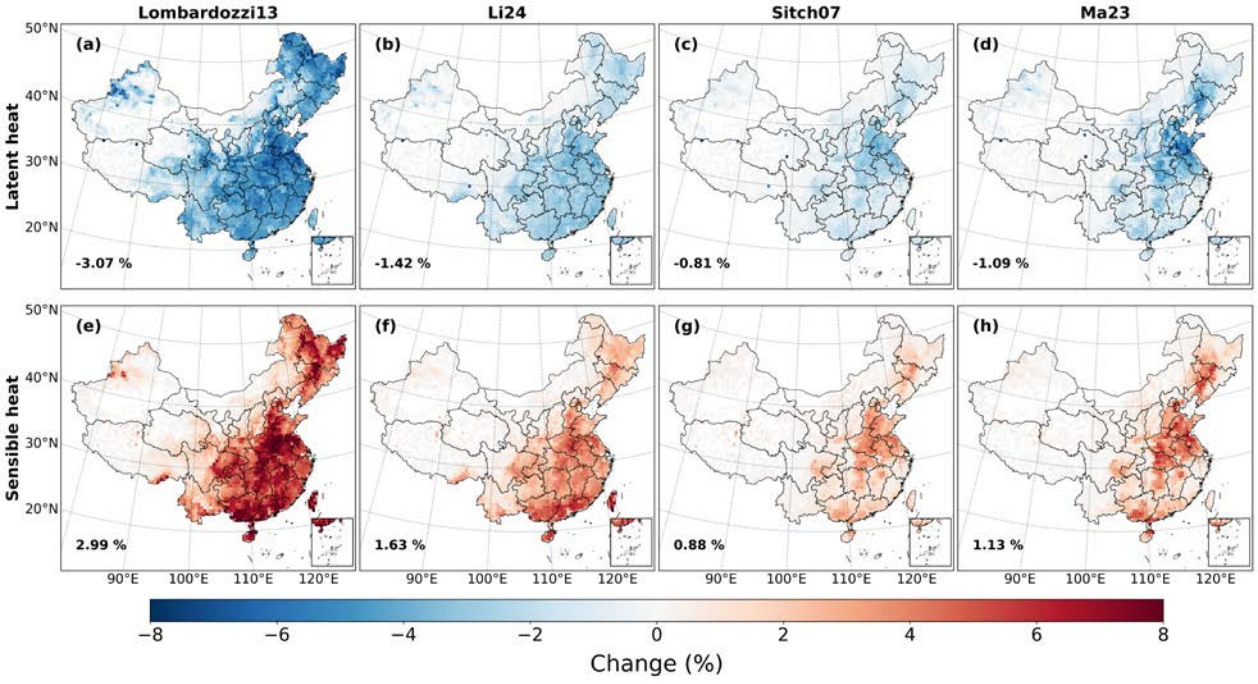


Figure 10. Same as Fig. 7, but for latent heat (LE) and sensible heat (H) fluxes.

3.4 Inter-Scheme Discrepancies in Ozone Impacts Across Plant Functional Types

PFT-level history outputs from the regional simulations reveal clear vegetation-dependent differences among schemes (Fig. 11). All schemes identified cropland as the most O_3-sensitive ecosystem across carbon, water, and energy fluxes, but rankings for other vegetation types diverged. Under Lombardozzi13, cropland GPP declined by 22.9%, followed by grass (18.0%), needleleaf trees (15.9%), broadleaf trees (12.0%), and shrubs (7.69%). The same cropland-led ordering appeared for transpiration, H, and LE, with cropland changes of −17.7%, +9.81%, and −7.26%, respectively.

Lombardozzi13 produced larger O_3 impacts than the other three schemes for all carbon, water, and energy variables and all PFTs. Needleleaf forests and shrubs responded strongly under Lombardozzi13 (GPP −15.9% and −7.69%; transpiration −11.8% and −3.75%) but weakly under Li24, Sitch07, and Ma23, where GPP reductions for these two PFTs remained below about 1.2%. Broadleaf forests responded more strongly under Lombardozzi13 and Li24 (GPP reductions of 12.0% and 6.75%) than under Sitch07 and Ma23 (about 1%). Energy-flux responses followed the same vegetation ranking: cropland showed the largest H increases and LE decreases in every scheme, while forest and shrub energy-flux changes were substantial mainly under Lombardozzi13 and, for broadleaf trees, under Li24.

Li24 showed pronounced PFT dependence and uncoupled GPP–transpiration responses. In grasslands, it reduced GPP by 10.1% but transpiration by only 1.54% (ratio ≈ 6.6), well above the 1.6–3.1 range of the other schemes. In needleleaf forests, Li24 reduced transpiration (2.51%) more than GPP (0.63%), a pattern not seen in the other schemes. Broadleaf forests under Li24 retained a more conventional coupling, with GPP and transpiration reductions of 6.75% and 5.15%. Correspondingly, Li24

https://doi.org/10.5194/egusphere-2026-5656
Preprint. Discussion started: 9 November 2026
© Author(s) 2026. CC BY 4.0 License.

produced clear cropland and broadleaf-tree signals in H and LE, but only weak grassland energy-flux changes despite the sizable grassland GPP loss.

Sitch07 and Ma23 produced similar PFT patterns, with synchronous GPP and transpiration changes and GPP reductions roughly 1–3 times those of transpiration. Forest and shrub impacts remained weak for both schemes. Cropland again dominated, with GPP reductions of 12.0% (Sitch07) and 11.4% (Ma23). Ma23, however, strengthened grassland impacts relative to Sitch07, with a GPP reduction of 15.7% versus 8.48%, and a parallel increase in grassland transpiration and LE responses. Thus scheme disagreement was largest for grasslands and needleleaf forests, whereas cropland sensitivity was robust across all four O_3 parameterizations.

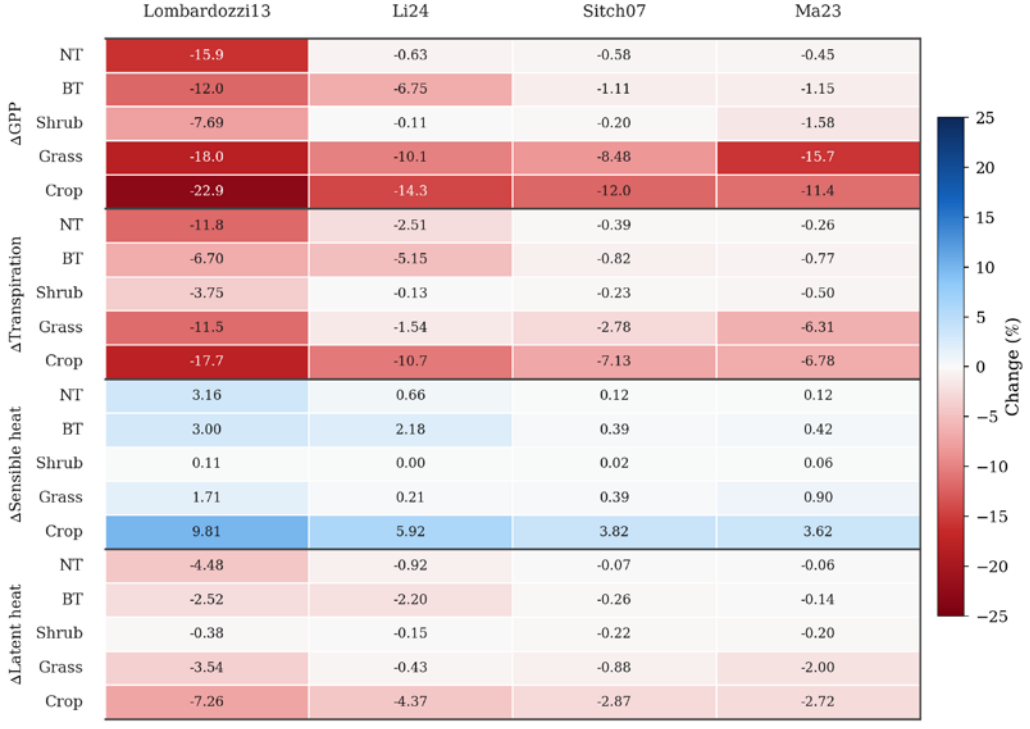


Figure 11. O_3 impacts on carbon, water, and energy fluxes across five plant functional types under the four schemes: needleleaf forest (NT), broadleaf forest (BT), shrub, grass, and crop. Rows are variables; columns are scenarios.

4 Discussion

Within a unified CLM5.0 framework, we compared four stomatal O_3 uptake schemes (Lombardozzi13, Li24, Sitch07, and Ma23) and assessed their effects on simulated carbon, water, and energy fluxes over China at site and regional scales. The schemes differ not only in quantified ecological O_3 effects but also in how they change model skill, and those skill changes do not map directly onto physiological realism. O_3 damage parameterization therefore remains a major uncertainty source in land surface model (LSM) assessments of O_3 impacts.

https://doi.org/10.5194/egusphere-2026-5656
Preprint. Discussion started: 9 November 2026
© Author(s) 2026. CC BY 4.0 License.

Zhou et al. (2026) primarily ranked ozone-stress schemes by GPP agreement with MODIS and FLUXNET. Although they noted that apparent skill depends on the host-model baseline, scheme preference was still inferred mainly from GPP metrics. Evaluating schemes solely with GPP skill, or even with GPP–transpiration–energy statistics alone, has clear limits. In our study, without O_3 damage, CLM5.0 already captures spatiotemporal patterns of carbon–water–energy fluxes over China reasonably well ($R^2 > 0.74$ for all variables), yet systematic biases remain, including underestimated GPP, transpiration, and LE in humid southern regions and slightly overestimated H over the Tibetan Plateau and western China. Once O_3 damage is added, scheme effects on skill depend on interactions between O_3 suppression and these background biases. If OFF overestimates GPP, moderate O_3 damage can reduce RMSE; if OFF already underestimates GPP or LE, O_3 damage worsens the bias. Because CLM5.0 underestimates LE in southern China, O_3-induced stomatal closure further lowers LE and raises H. Some schemes can therefore improve carbon-flux skill without improving energy-flux skill. LSM performance evaluation should therefore be separated from assessment of O_3 parameterizations. Refining damage schemes still requires independent constraints from fumigation experiments, physiological observations, and leaf-scale measurements. Because O_3 schemes affect both photosynthesis stomatal conductance, and thus transpiration and energy partitioning, evaluation should consider coupled carbon–water–energy responses rather than GPP alone.

With identical model structure and forcing, changing only the damage scheme can alter estimated ecological O3 effects over China by a factor of about 2–3. When comparisons are restricted to a common scheme formulation, published estimates of the relative magnitude of national or regional reductions in GPP and transpiration remain inconsistent. For Lombardozzi13 decoupled schemes, Cao et al. (2024) reported widespread transpiration declines exceeding −25% under L2013. In that study, fractional inhibition of GPP was weaker than that of transpiration. Jin et al. (2023), Zhu et al. (2022), and Lombardozzi13 in the present study more often indicate larger fractional reductions in GPP than in transpiration. For example, Jin et al. (2023) reported national reductions of −29.23% in GPP and −17.47% in transpiration. For Sitch07, Cao et al. (2024) obtained nearly identical summertime China-mean reductions in GPP and transpiration within WRF-Chem/Noah-MP. Reductions were approximately −5.5% for both fluxes under low sensitivity and −8.4% under high sensitivity. In contrast, the present CLM5.0 simulations yield a fractional GPP reduction of about −5.0%, roughly twice the corresponding reduction in transpiration (−2.3%). Accordingly, coupled schemes do not consistently yield similar fractional reductions in GPP and transpiration across studies. Decoupled schemes likewise do not consistently yield substantially larger fractional GPP losses than transpiration losses. These discrepancies may arise from host-model canopy resistance structure, online versus offline meteorology–chemistry coupling, O3 forcing, and vegetation dynamics. Existing literature remains insufficient to isolate their separate contributions. Cross-model diagnostics under harmonized scheme definitions will be required to constrain uncertainty in the GPP–transpiration ratio.

Scheme differences arise from how O_3 uptake and plant physiological regulation are represented. Lombardozzi13 builds damage functions from diurnal cumulative stomatal O_3 uptake and applies relatively uniform PFT parameters, allowing damage to intensify with cumulative exposure and potentially amplifying long-term effects. Li24 considers effective daytime uptake and uses PFT-specific nonlinear responses for photosynthesis and stomatal conductance, better capturing vegetation

https://doi.org/10.5194/egusphere-2026-5656
Preprint. Discussion started: 9 November 2026
© Author(s) 2026. CC BY 4.0 License.

differences in uptake capacity and regulation. In grasslands, Li24 reduces GPP by 10.1% but transpiration by only 1.54% (ratio ≈ 6.6), well above the other schemes (1.6–3.1). In needleleaf forests, it reduces transpiration more than GPP. Sitch07 and Ma23 rely on instantaneous uptake and assume synchronous inhibition of photosynthesis and stomatal conductance. Different O_3 parameterizations therefore change not only impact magnitude but also simulated carbon–water coupling, with strong vegetation-type dependence. How PFT physiological traits are represented is a key uncertainty in modelling ecological O_3 effects.

Several limitations remain. First, intrinsic LSM biases complicate scheme evaluation, so model outputs do not fully isolate parameterization performance. Second, the number of flux sites is limited, and representativeness across ecosystem types needs improvement. Third, all four schemes apply empirical corrections after leaf physiological iterations are completed. This a posteriori treatment does not embed O_3 damage in the joint optimisation of photosynthesis and stomatal conductance. Future work should develop process-coupled schemes that place O_3 damage inside the leaf physiological iteration, and combine multi-scale constraints from fumigation experiments, eddy-covariance fluxes, and leaf measurements while accounting for interactions with drought, nitrogen deposition, elevated CO_2, and phenology. Gong et al. (2020) further show that, in online ModelE2-YIBs coupling, stomatal inhibition can elevate eastern China surface O_3 through reduced dry deposition and transpiration-related meteorological adjustments (approximately +2.1 ppbv under high sensitivity). Such positive feedback alters the exposure used to estimate ecological damage. The present offline CLM5.0 experiments prescribe observation-constrained O_3 and therefore omit this pathway. Quantifying the net O_3–vegetation effect will require online multi-module coupling in addition to improved damage schemes. Such advances would reduce uncertainty in LSM simulations of ecological O_3 effects.

5 Conclusion

This study couples four stomatal O_3 damage schemes (Lombardozzi13, Li24, Sitch07, and Ma23) into the Community Land Model version 5.0 (CLM5.0) and evaluates their impacts on terrestrial carbon–water–energy fluxes over China. Using observation-constrained surface O_3 forcing, we compare the schemes at the site scale against ChinaFLUX observations, at the regional scale across China, and at the plant functional type (PFT) scale. The aim is not only to quantify scheme-to-scheme differences in ecological O_3 effects, but also to clarify how those differences propagate through coupled carbon, water, and energy responses.

The results show that scheme choice is a first-order control on simulated O_3 impacts. Relative to the no-damage control, damage intensities differ substantially among schemes, especially for gross primary productivity (GPP) and transpiration. At both site and regional scales, Lombardozzi13 produces the strongest damage, about 2.4–3.5 times that of the other schemes, with 2005–2020 national-mean reductions of 15.14% for GPP and 10.65% for transpiration. Li24, Sitch07, and Ma23 yield more moderate and mutually closer estimates. Spatial patterns of O_3 impacts are broadly consistent across schemes and are concentrated over eastern China, but the impact fields of Lombardozzi13 and Li24 are more continuous, whereas high-impact

https://doi.org/10.5194/egusphere-2026-5656
Preprint. Discussion started: 9 November 2026
© Author(s) 2026. CC BY 4.0 License.

zones in Sitch07 and Ma23 are more localised. At the PFT scale, contrasts are largest in forests: Lombardozzi13 overestimates forest damage overall; Li24 suppresses GPP and transpiration in broadleaf forests more strongly than Sitch07 and Ma23, while its responses in needleleaf forests and shrubs resemble the latter two. Li24 also produces asynchronous GPP–transpiration responses across vegetation types, whereas Sitch07 and Ma23 remain more synchronous across most PFTs, except that Ma23 increases grassland sensitivity. These PFT-dependent contrasts indicate that ozone parameterizations change not only impact magnitude but also simulated carbon–water coupling.

Including O_3 damage generally reduces model skill relative to the no-damage control. However, these skill changes are entangled with CLM5.0 background biases: where the control overestimates GPP, moderate O_3 suppression can appear to improve RMSE, whereas where GPP or latent heat is already underestimated, O_3 damage further degrades performance and can worsen energy-flux biases. Skill metrics should therefore not be taken as direct evidence of scheme superiority. LSM performance evaluation needs to be separated from O_3-scheme evaluation, and scheme adequacy still requires independent constraints from fumigation experiments, physiological observations, and leaf-scale measurements.

Several boundaries remain. Intrinsic LSM biases, the limited number of flux sites, and the a posteriori implementation of all four schemes after leaf physiological iteration prevent a fully isolated ranking of parameterization realism. Future work should embed O_3 damage within the leaf physiological iteration, strengthen multi-scale observational constraints, and quantitatively separate the contributions of scheme structure, O_3 concentration fields, and host-model bias. Such advances are needed to reduce uncertainty in land surface assessments of ecological O_3 effects in China and to support more robust applications in air-pollution and ecosystem management.

Code and data availability

The modified CLM5.0 code for the four stomatal ozone damage schemes (Lombardozzi13, Li24, Sitch07, and Ma23) is available at https://doi.org/10.5281/zenodo.21670501 (Lin, 2026a). The simulation outputs underlying this study are available at https://doi.org/10.5281/zenodo.21696141 (Lin, 2026b). The code of the Earth system model CESM2.2.0 is archived at https://doi.org/10.5281/zenodo.11229776 (CESM Team, 2024). Site meteorological and flux data were obtained from the National Ecosystem Science Data Center, National Science & Technology Infrastructure of China (http://www.nesdc.org.cn; Yu et al., 2006). Regional meteorological forcing was obtained from the China Meteorological Forcing Dataset (CMFD, v2.0) (He et al., 2024) (https://doi.org/10.11888/Atmos.tpdc.302088). Surface ozone concentrations were obtained from HrSOD (Zhang et al., 2022) (https://doi.org/10.5281/zenodo.7415326). Spatial LMA fields were derived from the SLA dataset of Moreno-Martínez et al. (2018) (https://doi.org/10.1016/j.rse.2018.09.006). FLUXCOM carbon and energy fluxes are documented in Jung et al. (2019, 2020) (https://doi.org/10.1038/s41597-019-0076-8; https://doi.org/10.5194/bg-17-1343-2020). GLEAM transpiration data are documented in Miralles et al. (2011, 2025) (https://doi.org/10.5194/hess-15-453-2011; https://doi.org/10.1038/s41597-025-04610-y).

https://doi.org/10.5194/egusphere-2026-5656
Preprint. Discussion started: 9 November 2026
© Author(s) 2026. CC BY 4.0 License.

Author contributions

TC and XY conceived the study, determined the research direction, and supervised the project. XL performed the primary research, conducted the model simulations, and wrote the initial draft of the manuscript. SZ and SW assisted with data processing, formal analysis, and data visualization. TC and XY provided critical feedback on the methodology, discussed the results, and thoroughly revised the manuscript. All authors reviewed and approved the final manuscript.

Competing interests

The authors declare that they have no conflict of interest.

Disclaimer

Copernicus Publications adds a standard disclaimer: “Copernicus Publications remains neutral with regard to jurisdictional claims made in the text, published maps, institutional affiliations, or any other geographical representation in this paper. While Copernicus Publications makes every effort to include appropriate place names, the final responsibility lies with the authors. Views expressed in the text are those of the authors and do not necessarily reflect the views of the publisher.”

Acknowledgements

We acknowledge the financial support provided by our funding sources. We also thank the editors and reviewers for their valuable feedback on the revisions.

Financial support

This study is funded by the Qinghai Provincial Natural Science Foundation (2023-QLGKLYCZX-010, 2023-QLGKLYCZX-005, 2025-QLGKLYCZX-005), the National Natural Science Foundation of China (42130506, and 42161144003).

References

Ainsworth, E. A., Yendrek, C. R., Sitch, S., Collins, W. J., and Emberson, L. D.: The effects of tropospheric ozone on net primary productivity and implications for climate change, Annu. Rev. Plant Biol., 63, 637–661, https://doi.org/10.1146/annurev-arplant-042110-103829, 2012.

Anav, A., Menut, L., Khvorostyanov, D., and Viovy, N.: Impact of tropospheric ozone on the Euro-Mediterranean vegetation, Glob. Change Biol., 17, 2342–2359, https://doi.org/10.1111/j.1365-2486.2010.02387.x, 2011.

https://doi.org/10.5194/egusphere-2026-5656
Preprint. Discussion started: 9 November 2026
© Author(s) 2026. CC BY 4.0 License.

Ball, J. T., Woodrow, I. E., and Berry, J. A.: A model predicting stomatal conductance and its contribution to the control of photosynthesis under different environmental conditions, in: Progress in Photosynthesis Research, Vol. 4, edited by: Biggins, J., Martinus Nijhoff Publishers, Dordrecht, 221–224, https://doi.org/10.1007/978-94-017-0519-6_48, 1987.

Cao, J., Yue, X., and Ma, M.: Simulation of ozone–vegetation coupling and feedback in China using multiple ozone damage schemes, Atmos. Chem. Phys., 24, 3973–3987, https://doi.org/10.5194/acp-24-3973-2024, 2024.

Cen, X., He, N., Van Sundert, K., Terrer, C., Yu, K., Li, M., Xu, L., He, L., and Butterbach-Bahl, K.: Global patterns of nitrogen saturation in forests, One Earth, 8, 101132, https://doi.org/10.1016/j.oneear.2024.10.007, 2025.

Chen, H., Li, D., Gurmesa, G. A., Yu, G., Li, L., Zhang, W., Fang, H., and Mo, J.: Effects of nitrogen deposition on carbon cycle in terrestrial ecosystems of China: a meta-analysis, Environ. Pollut., 206, 352–360, https://doi.org/10.1016/j.envpol.2015.07.033, 2015.

Emberson, L. D., Ashmore, M. R., Cambridge, H. M., Simpson, D., and Tuovinen, J.-P.: Modelling stomatal ozone flux across Europe, Environ. Pollut., 109, 403–413, https://doi.org/10.1016/S0269-7491(00)00043-9, 2000.

Farquhar, G. D., von Caemmerer, S., and Berry, J. A.: A biochemical model of photosynthetic CO_2 assimilation in leaves of C_3 species, Planta, 149, 78–90, https://doi.org/10.1007/BF00386231, 1980.

Feng, Z., Xu, Y., Kobayashi, K., Dai, L., Zhang, T., Agathokleous, E., Calatayud, V., Paoletti, E., Mukherjee, A., Agrawal, M., Park, R. J., Oak, Y. J., and Yue, X.: Ozone pollution threatens the production of major staple crops in East Asia, Nat. Food, 3, 47–56, https://doi.org/10.1038/s43016-021-00422-6, 2022.

Fu, Y., Yu, G., Wang, Y., Li, Z., and Hao, Y.: Effect of water stress on ecosystem photosynthesis and respiration of a Leymus chinensis steppe in Inner Mongolia, Sci. China Ser. D-Earth Sci., 49, 196–206, https://doi.org/10.1007/s11430-006-8196-3, 2006.

Gong, C., Lei, Y., Ma, Y., Yue, X., and Liao, H.: Ozone–vegetation feedback through dry deposition and isoprene emissions in a global chemistry–carbon–climate model, Atmos. Chem. Phys., 20, 3841–3857, https://doi.org/10.5194/acp-20-3841-2020, 2020.

He, J., Yang, K., Tang, W., Lu, H., Qin, J., Chen, Y., and Li, X.: The first high-resolution meteorological forcing dataset for land process studies over China, Sci. Data, 7, 25, https://doi.org/10.1038/s41597-020-0369-y, 2020.

He, J., Yang, K., Li, X., Tang, W., Shao, C., Jiang, Y., and Ding, B.: China meteorological forcing dataset v2.0 (1951–2024), National Tibetan Plateau / Third Pole Environment Data Center [data set], https://doi.org/10.11888/Atmos.tpdc.302088, 2024.

Hu, Z., Yu, G., Fu, Y., Sun, X., Li, Y., Shi, P., Wang, Y., and Zheng, Z.: Effects of vegetation control on ecosystem water use efficiency within and among four grassland ecosystems in China, Glob. Change Biol., 14, 1609–1619, https://doi.org/10.1111/j.1365-2486.2008.01582.x, 2008.

Jin, Z., Yan, D., Zhang, Z., Li, M., Wang, T., Huang, X., Xie, M., Li, S., and Zhuang, B.: Effects of elevated ozone exposure on regional meteorology and air quality in China through ozone–vegetation coupling, J. Geophys. Res.-Atmos., 128, e2022JD038119, https://doi.org/10.1029/2022JD038119, 2023.

https://doi.org/10.5194/egusphere-2026-5656
Preprint. Discussion started: 9 November 2026
© Author(s) 2026. CC BY 4.0 License.

Jung, M., Koirala, S., Weber, U., Ichii, K., Gans, F., Camps-Valls, G., Papale, D., Schwalm, C., Tramontana, G., and Reichstein, M.: The FLUXCOM ensemble of global land-atmosphere energy fluxes, Sci. Data, 6, 74, https://doi.org/10.1038/s41597-019-0076-8, 2019.

Jung, M., Schwalm, C., Migliavacca, M., Walther, S., Camps-Valls, G., Koirala, S., Anthoni, P., Besnard, S., Bodesheim, P., Carvalhais, N., Chevallier, F., Gans, F., Goll, D. S., Haverd, V., Kohler, P., Ichii, K., Jain, A. K., Liu, J., Lombardozzi, D., Nabel, J. E. M. S., Nelson, J. A., O'Sullivan, M., Pallandt, M., Papale, D., Peters, W., Pongratz, J., Roedenbeck, C., Sitch, S., Tramontana, G., Walker, A., Weber, U., and Reichstein, M.: Scaling carbon fluxes from eddy covariance sites to globe: synthesis and evaluation of the FLUXCOM approach, Biogeosciences, 17, 1343–1365, https://doi.org/10.5194/bg-17-1343-2020, 2020.

Krupa, S. V. and Manning, W. J.: Atmospheric ozone: formation and effects on vegetation, Environ. Pollut., 50, 101–137, https://doi.org/10.1016/0269-7491(88)90187-X, 1988.

Lawrence, D. M., Fisher, R. A., Koven, C. D., Oleson, K. W., Swenson, S. C., Bonan, G., Collier, N., Ghimire, B., van Kampenhout, L., Kennedy, D., Kluzek, E., Lawrence, P. J., Li, F., Li, H., Lombardozzi, D., Riley, W. J., Sacks, W. J., Shi, M., Vertenstein, M., Wieder, W. R., Xu, C., Ali, A. A., Badger, A. M., Bisht, G., van den Broeke, M., Brunke, M. A., Burns, S. P., Buzan, J., Clark, M., Craig, A., Dahlin, K., Drewniak, B., Fisher, J. B., Flanner, M., Fox, A. M., Gentine, P., Hoffman, F., Keppel-Aleks, G., Knox, R., Kumar, S., Lenaerts, J., Leung, L. R., Lipscomb, W. H., Lu, Y., Pandey, A., Pelletier, J. D., Perket, J., Randerson, J. T., Ricciuto, D. M., Sanderson, B. M., Slater, A., Subin, Z. M., Tang, J., Thomas, R. Q., Val Martin, M., and Zeng, X.: The Community Land Model version 5: description of new features, benchmarking, and impact of forcing uncertainty, J. Adv. Model. Earth Syst., 11, 4245–4287, https://doi.org/10.1029/2018MS001583, 2019.

Li, F., Zhou, Z., Levis, S., Sitch, S., Hayes, F., Feng, Z., Reich, P. B., Zhao, Z., and Zhou, Y.: Quantifying the role of ozone-caused damage to vegetation in the Earth system: a new parameterization scheme for photosynthetic and stomatal responses, Geosci. Model Dev., 17, 6173–6193, https://doi.org/10.5194/gmd-17-6173-2024, 2024.

Li, K., Jacob, D. J., Liao, H., Shen, L., Zhang, Q., and Bates, K. H.: Anthropogenic drivers of 2013–2017 trends in summer surface ozone in China, Proc. Natl. Acad. Sci. U.S.A., 116, 422–427, https://doi.org/10.1073/pnas.1812168116, 2019.

Li, L., Qiu, B., Zhao, S., Miao, X., Chen, C., Chen, J., Ni, Y., Huang, X., Chen, H., and Guo, W.: Integrating ozone–vegetation damage schemes into SSiB4/TRIFFID: evaluation of six parameterizations and refinement of ozone decay process across plant functional types, EGUsphere [preprint], https://doi.org/10.5194/egusphere-2026-1335, 2026.

Lombardozzi, D., Sparks, J. P., and Bonan, G.: Integrating O_3 influences on terrestrial processes: photosynthetic and stomatal response data available for regional and global modeling, Biogeosciences, 10, 6815–6831, https://doi.org/10.5194/bg-10-6815-2013, 2013.

Lin, X.: Four modified stomatal ozone damage schemes coupled into CLM5.0 for vegetation carbon–water–energy simulations, Zenodo [code], https://doi.org/10.5281/zenodo.21670501, 2026a.

Lin, X.: CLM5.0 simulation outputs for four stomatal ozone damage schemes over China, Zenodo [data set], https://doi.org/10.5281/zenodo.21696141, 2026b.

https://doi.org/10.5194/egusphere-2026-5656
Preprint. Discussion started: 9 November 2026
© Author(s) 2026. CC BY 4.0 License.

Lombardozzi, D., Levis, S., Bonan, G., Hess, P. G., and Sparks, J. P.: The influence of chronic ozone exposure on global carbon and water cycles, J. Clim., 28, 292–305, https://doi.org/10.1175/JCLI-D-14-00223.1, 2015.

Lu, X., Hong, J., Zhang, L., Cooper, O. R., Schultz, M. G., Xu, X., Wang, T., Gao, M., Zhao, Y., and Zhang, Y.: Severe surface ozone pollution in China: a global perspective, Environ. Sci. Technol. Lett., 5, 487–494, https://doi.org/10.1021/acs.estlett.8b00366, 2018.

Ma, Y., Yue, X., Sitch, S., Unger, N., Uddling, J., Mercado, L. M., Gong, C., Feng, Z., Yang, H., Zhou, H., Tian, C., Cao, Y., Lei, Y., Cheesman, A. W., Xu, Y., and Duran Rojas, M. C.: Implementation of trait-based ozone plant sensitivity in the Yale Interactive terrestrial Biosphere model v1.0 to assess global vegetation damage, Geosci. Model Dev., 16, 2261–2276, https://doi.org/10.5194/gmd-16-2261-2023, 2023.

Mao, J., Tai, A. P. K., Yung, D. H. Y., Yuan, T., Chau, K. T., and Feng, Z.: Multidecadal ozone trends in China and implications for human health and crop yields: a hybrid approach combining a chemical transport model and machine learning, Atmos. Chem. Phys., 24, 345–366, https://doi.org/10.5194/acp-24-345-2024, 2024.

Mills, G., Pleijel, H., Braun, S., Büker, P., Bermejo, V., Calvo, E., Danielsson, H., Emberson, L., Fernández, I. G., Grünhage, L., Harmens, H., Hayes, F., Karlsson, P.-E., and Simpson, D.: New stomatal flux-based critical levels for ozone effects on vegetation, Atmos. Environ., 45, 5064–5068, https://doi.org/10.1016/j.atmosenv.2011.06.009, 2011.

Miralles, D. G., Holmes, T. R. H., De Jeu, R. A. M., Gash, J. H., Meesters, A. G. C. A., and Dolman, A. J.: Global land-surface evaporation estimated from satellite-based observations, Hydrol. Earth Syst. Sci., 15, 453–469, https://doi.org/10.5194/hess-15-453-2011, 2011.

Miralles, D. G., Bonte, O., Koppa, A., Baez-Villanueva, O. M., Tronquo, E., Zhong, F., Beck, H. E., Hulsman, P., Dorigo, W. A., Verhoest, N. E. C., and Haghdoost, S.: GLEAM4: global land evaporation and soil moisture dataset at 0.1° resolution from 1980 to near present, Sci. Data, 12, 416, https://doi.org/10.1038/s41597-025-04610-y, 2025.

Moreno-Martínez, Á., Camps-Valls, G., Kattge, J., Robinson, N., Reichstein, M., van Bodegom, P., Kramer, K., Cornelissen, J. H. C., Reich, P., Bahn, M., Niinemets, Ü., Peñuelas, J., Craine, J. M., Cerabolini, B. E. L., Minden, V., Laughlin, D. C., Sack, L., Allred, B., Baraloto, C., Byun, C., Soudzilovskaia, N. A., and Running, S. W.: A methodology to derive global maps of leaf traits using remote sensing and climate data, Remote Sens. Environ., 218, 69–88, https://doi.org/10.1016/j.rse.2018.09.006, 2018.

Moriasi, D. N., Arnold, J. G., Van Liew, M. W., Bingner, R. D., Harmel, R. D., and Veith, T. L.: Model evaluation guidelines for systematic quantification of accuracy in watershed simulations, Trans. ASABE, 50, 885–900, https://doi.org/10.13031/2013.23153, 2007.

Sitch, S., Cox, P. M., Collins, W. J., and Huntingford, C.: Indirect radiative forcing of climate change through ozone effects on the land-carbon sink, Nature, 448, 791–794, https://doi.org/10.1038/nature06059, 2007.

Sun, X.-M., Zhu, Z.-L., Wen, X.-F., Yuan, G.-F., and Yu, G.-R.: The impact of averaging period on eddy fluxes observed at ChinaFLUX sites, Agric. For. Meteorol., 137, 188–193, https://doi.org/10.1016/j.agrformet.2006.02.012, 2006.

https://doi.org/10.5194/egusphere-2026-5656
Preprint. Discussion started: 9 November 2026
© Author(s) 2026. CC BY 4.0 License.

Taylor, K. E.: Summarizing multiple aspects of model performance in a single diagram, J. Geophys. Res.-Atmos., 106, 7183–7192, https://doi.org/10.1029/2000JD900719, 2001.

Wang, T., Xue, L., Brimblecombe, P., Lam, Y. F., Li, L., and Zhang, L.: Ozone pollution in China: a review of concentrations, meteorological influences, chemical precursors, and effects, Sci. Total Environ., 575, 1582–1596, https://doi.org/10.1016/j.scitotenv.2016.10.081, 2017.

Wang, W., Parrish, D. D., Wang, S., Bao, F., Ni, R., Li, X., Yang, S., Wang, H., Cheng, Y., and Su, H.: Long-term trend of ozone pollution in China during 2014–2020: distinct seasonal and spatial characteristics and ozone sensitivity, Atmos. Chem. Phys., 22, 8935–8949, https://doi.org/10.5194/acp-22-8935-2022, 2022.

Wang, Q., Huang, M., Wang, S., Chen, B., Liu, Z., Wang, Z., Chen, S., Li, H., Zhu, T., Li, D., Li, Y., Lin, H., and Sun, L.: Evaluation of the impacts of ozone on the vegetation productivity of woodland and grassland ecosystems in China, Ecol. Model., 483, 110426, https://doi.org/10.1016/j.ecolmodel.2023.110426, 2023.

Willmott, C. J. and Matsuura, K.: Advantages of the mean absolute error (MAE) over the root mean square error (RMSE) in assessing average model performance, Clim. Res., 30, 79–82, https://doi.org/10.3354/cr030079, 2005.

Xie, X., Wang, T., Yue, X., Li, S., Zhuang, B., Wang, M., and Yang, X.: Numerical modeling of ozone damage to plants and its effects on atmospheric CO_2 in China, Atmos. Environ., 217, 116970, https://doi.org/10.1016/j.atmosenv.2019.116970, 2019.

Xie, N., Wang, T., Li, S., Zhuang, B., Li, M., Xie, M., Zhang, Q., Ma, D., Liu, J., Chen, J. M., Feng, Z., Melas, D., and Karatzas, K.: Dissimilar roles of aerosols, nitrogen deposition and ozone on the terrestrial carbon sink in China during 2010–2020, Atmos. Chem. Phys., 26, 5925–5945, https://doi.org/10.5194/acp-26-5925-2026, 2026.

Yu, G.-R., Wen, X.-F., Sun, X.-M., Tanner, B. D., Lee, X., and Chen, J.-Y.: Overview of ChinaFLUX and evaluation of its eddy covariance measurement, Agric. For. Meteorol., 137, 125–137, https://doi.org/10.1016/j.agrformet.2006.02.011, 2006.

Yu, G., Song, X., Wang, Q., Liu, Y., Guan, D., Yan, J., Sun, X., Zhang, L., and Wen, X.: Water-use efficiency of forest ecosystems in eastern China and its relations to climatic variables, New Phytol., 177, 927–937, https://doi.org/10.1111/j.1469-8137.2007.02316.x, 2008.

Yue, X. and Unger, N.: The Yale Interactive terrestrial Biosphere model version 1.0: description, evaluation and implementation into NASA GISS ModelE2, Geosci. Model Dev., 8, 2399–2417, https://doi.org/10.5194/gmd-8-2399-2015, 2015.

Yue, X., Unger, N., Harper, K., Xia, X., Liao, H., Zhu, T., Xiao, J., Feng, Z., and Li, J.: Ozone and haze pollution weakens net primary productivity in China, Atmos. Chem. Phys., 17, 6073–6089, https://doi.org/10.5194/acp-17-6073-2017, 2017.

Yue, X., Zhou, H., Tian, C., Ma, Y., Hu, Y., Gong, C., Zheng, H., and Liao, H.: Development and evaluation of the interactive Model for Air Pollution and Land Ecosystems (iMAPLE) version 1.0, Geosci. Model Dev., 17, 4621–4642, https://doi.org/10.5194/gmd-17-4621-2024, 2024.

Zhang, W., Liu, D., and Shi, H.: Hourly Surface Ozone data (HrSOD) across China during 2005–2020, Zenodo [data set], https://doi.org/10.5281/zenodo.7415326, 2022.

https://doi.org/10.5194/egusphere-2026-5656
Preprint. Discussion started: 9 November 2026
© Author(s) 2026. CC BY 4.0 License.



595 Zhu, J., Tai, A. P. K., and Yim, S. H. L.: Effects of ozone–vegetation interactions on meteorology and air quality in China using a two-way coupled land–atmosphere model, Atmos. Chem. Phys., 22, 765–782, https://doi.org/10.5194/acp-22-765-2022, 2022.